Research on the High Permeability Permalloy and its Application to the Hydrogen Maser

Wujiabei Xu*†, Xueling Hou*, Tao Lu‡, Zijie Jiao*,Xiaotong Xu*, Jiayu Dai†

Email: xwjb@shao.ac.cn, flybird1656@163.com, freedomhorse@163.com, jiao_zj@163.com, 1345507880@qq.com, daijy@shao.ac.cn

* School of Materials Science and Engineering, Shanghai University, Shanghai, China
†Time & Frequency Research Laboratory, Shanghai Astronomical Observatory, Chinese Academy of Sciences, Shanghai, China
‡Shanghai Kingv Material Technology Co.,Ltd

***Abstract*—The hydrogen maser works by using the transition between the two energy levels of hydrogen atoms. The energy levels vary with the ambient magnetic fields. The magnetic shielding system is important to frequency instability performance of hydrogen maser, and the improvement can be realized by two parts: material research and structure optimization. Therefore, the permalloy $Fe_{15}Ni_{80}Mo_{(5-x)}Si_x$ (x=0,1,2,3) was developed through melting, rolling, annealing and other steps. Then the relevant parameters were measured, and the simulations were carried out accordingly. In general, $Fe_{15}Ni_{80}Mo_4Si_1$ has the best magnetic property, such as its maximum permeability being 407,584 and the relatively large size grain with a uniform distribution. The crystalline phase is mainly $FeNi_3$. The magnetic shielding coefficient can reach 1.5×10^9 by simulations, with the measured permeability.**

Keywords—Hydrogen Maser; Magnetic Shielding; Simulation; Permalloy

I. INTRODUCTION

The hydrogen maser uses the hyperfine energy level transition signal of ground state hydrogen atom from (F = 1, m_F = 0) state to (F = 0, m_F = 0) state to lock the crystal oscillator to achieve the stability of the whole machine frequency signal. The frequency stability can reach (10^{-15}~10^{-16})/(10^3~10^4 s), mainly used in aerospace and local timing fields. At present, the long-term frequency stability of the hydrogen maser in orbit[1] can reach 3×10^{-15} /day, and the frequency drift rate is less than 5×10^{-15} /day.

As shown in Fig.1(a)[2], the hyperfine magnetic energy level of hydrogen atom is related to the magnetic field, the stability of the hydrogen maser is closely related to the magnetic field size. In order to make the output frequency less sensitive to the magnetic field and improve the stability of the hydrogen maser, the magnetic field size should not be too large. When the frequency stability of the hydrogen maser frequency scale is improved to (10^{-16}-10^{-17}) /day, magnetic shielding is very important.

At present, the main magnetic shielding materials used in hydrogen masers are permalloy. Permalloy is an Fe-Ni alloy, which Ni content 30-90%, with high permeability and low coercivity characteristics, the current magnetic shielding material is 1J85 ($Ni_{85}Fe_{15}$), and then in the original system, the element Mo was added, and $Ni_{80}Fe_{15}Mo_5$ is now used as a component of 1J85.

For the addition of Mo element, it has been pointed out [3,4] that the μ((Fe, Ni)$_7$Mo$_6$) phase generated during the aging process of Fe-Mo-Ni alloy enhances the magnetic properties.

For the heat treatment of permalloy, the reduction of the number of voids in the amorphous structure and the weakening of stress anisotropy mean that the residual stress released after heat treatment can increase the permeability. At the same time, the appropriate annealing process also affects the grain size and the uniformity of soft magnetic phase. Lei et al. [5] divided cooling into slow cooling and fast cooling in the process of trying, and finally concluded that for DC magnetic properties, the best heat treatment process is to hold heat at 1180 °C for 5 h, then cool down to 510 °C at 100 °C /min and hold heat for 1 h, and then cool down to 200 °C at 250 °C /h.

Fig.1(b)[6] shows the structure of the active hydrogen frequency standard, in which the magnetic shielding system consists of four layers of coaxial magnetic shielding shells, which are mainly used to shield the interference of the environmental magnetic field on the atomic transition. Generally, in the absence of other electromagnetic equipment interference sources, the geomagnetic field will also affect the hyperfine energy level of the atom.

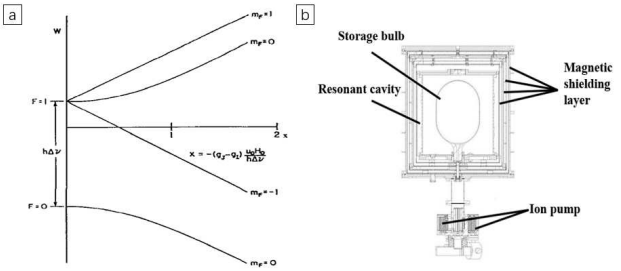

Fig. 1. (a) Hydrogen atom transition spectrum (b) Schematic diagram of hydrogen maser structure

At present, the magnetic shielding performance of hydrogen frequency is mainly improved through two aspects of material and structure: (1) 1J85 alloy has promotion space in lower magnetic field; (2) Optimize the design of magnetic shielding and improve the shielding coefficient. Therefore, we made our own new 1J85 alloy and compared it with other 1J85 alloys on the market.

II. EXPERIMENT

A. Sample Preparation

According to the proportion of elements contained in $Fe_{15}Ni_{80}Mo_{(5-x)}Si_x$(x=0,1,2,3) Permalloy ingredients. The raw

the National Natural Science Foundation of China (Grants No. 12373078).

material supplier is Zhongnuo New Material (Beijing) Technology Co., LTD. Wk-II type non-consumable vacuum arc furnace was used to melt 40g molten ingot. The molten ingot is heated to 600 °C, and then pressed to a cake shape with a diameter greater than 35 mm by a hydraulic press, then put the alloy in the sand to accelerate cooling. To achieve the needs of the ring sample, the ring is machined to 20*16*y (x=0.5, 1,2) mm and 30*24*y mm using a lathe. Then it needs heat treatment, the heat treatment process is to hold the heat at 1180 °C for 5h, and reduce the temperature to 500 °C at the speed of 150 °C /h, and then cool the heat at 500 °C for 1h, and then air cooling.

B. Characterization and Testing

XRD pattern using Malvern Panalytical Empyrean X-ray diffractometer (Cu target, Kα rays). The DC performance parameters of soft magnetic materials were measured by FE-2100SD DC test system produced by Hunan Yongyi Technology Co., LTD. DM300 field emission scanning electron microscope produced by PHENOM Company was used to observe the surface microstructure of the sample.

III. RESULTS AND DISCUSSION

A. Soft Magnetic Performance

Fig.2(a) and (b) respectively show the hysteresis loop and magnetization curve of the applied materials, including $Fe_{15}Ni_{80}Mo_{(5-x)}Si_x$(x=0,1,2,3), and the composition of 1J85 is $Fe_{14}Ni_{80}Mo_5Si_{0.5}Mn_{0.5}$, where 1J85-1 is the sample prepared by individuals imitating market ingredients. 1J85-2 is the material being used in the laboratory. Important parameters are shown in Table I. For magnetic properties, permeability is the main reference index of magnetic shielding materials. When Si=1, the maximum permeability μ_m of the material reaches a maximum value of 407584, which is 321% of the permeability of the material currently being applied, compared with 154 % for 1J85-1. At present, China's performance requirements for 1J85 are permeability ≥225000, so the permeability of Si=1 material is higher than the performance of conventional 1J85 materials in the domestic market, and the magnetic field size corresponding to the maximum permeability of all materials is about 1 A/m. In terms of saturation magnetic induction intensity B_s, when Si=0, the material's Bs reaches the maximum value, and the larger B_s means the maximum magnetic field that the material can apply. For magnetic shielding of hydrogen frequency, the Bs of all materials is much larger than the geomagnetic field. Remanent B_r means how much magnetic field remains in the material after demagnetization. Si=2 and 1J85-2 have better properties. Coercive force is 1J85-2 performance is better. After comprehensive comparison, the performance of $Fe_{15}Ni_{80}Mo_4Si_1$ is more in line with the needs of improving the performance of magnetic shield systems.

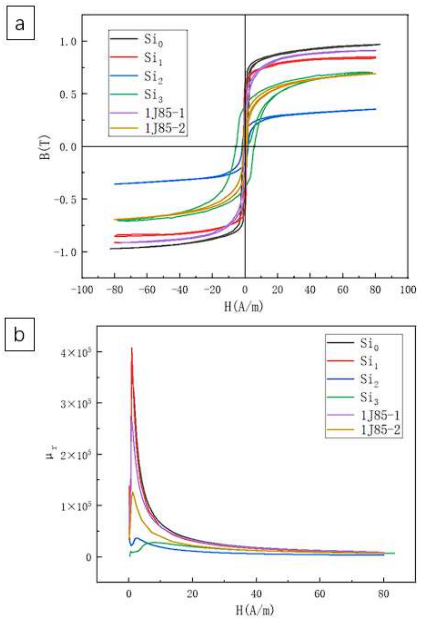

Fig. 2. $Fe_{15}Ni_{80}Mo_{(5-x)}Si_x$ (x= 0,1,2,3) and 1J85 (a) hysteresis loop (b) magnetization curve $Fe_{15}Ni_{80}Mo_{(5-x)}Si_x$ (x= 0,1,2,3) and 1J85

TABLE I. MAGNETIC PROPERTIES

Material	μ_i	μ_m	B_s(T)	B_r(T)	H_c(A/m)
Si_0	79197	361713	1	0.3956	1
Si_1	48092	407584	0.8	0.6	0.8
Si_2	21905	36944	0.4	0.2	1.7
Si_3	1975	28226	0.9	0.4	5.7
1J85-1	59683	264517	0.9	0.4	0.7
1J85-2	40650	126915	0.7	0.2	0.4

B. Microstructure

Fig.3 shows the SEM images of each material. In $Fe_{15}Ni_{80}Mo_{(5-x)}Si_x$(x=0,1,2,3), with the increase of Si content, the grains become coarser and more twin structures appear at the same time. When Si=2, although the number of large grains increases, some small grains appear, resulting in poor uniformity. Therefore, less Si can promote grain growth, and with the further increase of Si content, as a non-Feni3 phase Si element, itself will become a nucleation site, resulting in more small grains that are not conducive to magnetic properties of the material.

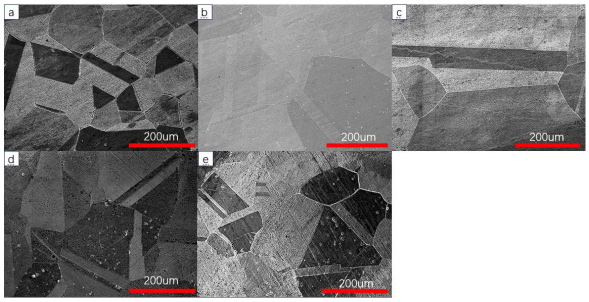

Fig. 3. SEM of $Fe_{15}Ni_{80}Mo_{(5-x)}Si_x$ (a) Si=0 (b) Si=1 (c) Si=2 (d) Si=3 (e) 1J85-2

C. XRD

Fig.4 shows the XRD pattern of $Fe_{15}Ni_{80}Mo_{(5-x)}Si_x$(x=0,1,2,3), with peaks representing the $FeNi_3$ phase. $FeNi_3$ phase is the main paramagnetic property of 1J85, and the addition of Si does not change the phase composition. The diffraction peak position of each alloy is the same, and all are $FeNi_3$ phase (111), (200), (220), (311), (222) crystal faces. From the point of view of peak strength, with the increase of Si content, the diffraction peak intensity of (200) and (220) first increases and then decreases, indicating that the grain of (200) and (220) orientation grows preferentially[7,8].

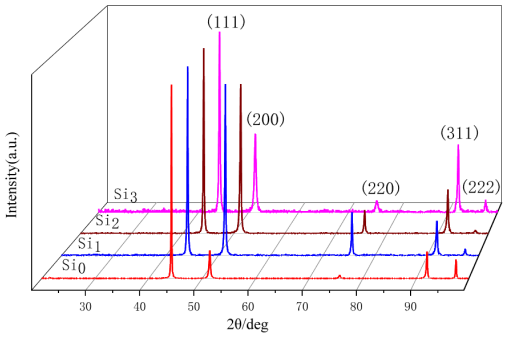

Fig. 4. XRD of $Fe_{15}Ni_{80}Mo_{(5-x)}Si_x$

IV. SIMULATION

A. Model Introduction

Fig. 5 (a) shows the longitudinal cross-section diagram of the two-dimensional axisymmetric model of the hydrogen frequency standard simulation model, with air domain, four layers of magnetic shielding and storage bubble successively from outside to inside. Fig. 5(b) The distribution of the magnetic field measured in the laboratory, with the maximum magnetic field strength in the longitudinal direction (40 μT) in line with the distribution of the geomagnetic field, and in practical applications there will be holes, resulting in magnetic leakage, so the longitudinal direction is the main direction of investigation. Fig. 5(c) shows the distribution of the magnetic field without magnetic shielding, and the size and direction of the magnetic field in the spatial domain are the same as the laboratory test results.

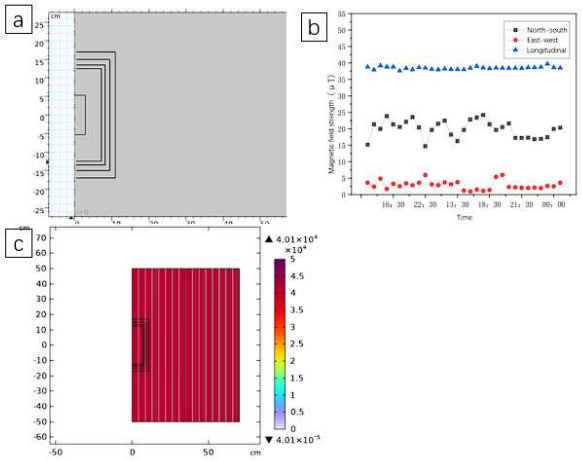

Fig. 5. (a) two-dimensional axisymmetric model (b) ambient magnetic field distribution in the laboratory (c) magnetic field distribution without magnetic shielding

B. Magnetic Shielding Effect under Different Permeability

Fig. 6 shows the magnetic field distribution in the storage bubble region under different permeability. It can be seen that as the permeability increases, the reduction rate of the internal magnetic field decreases continuously. At low permeability, the central magnetic field is greater than the surrounding magnetic field, while at high permeability, it is the opposite. The flow line in the figure is isoline. With the increase of permeability, the flow line distribution becomes more sparse and tends to move outward, indicating that the magnetic field line is mainly concentrated inside the magnetic shielding material. The specific values are shown in Table II, and the calculation formula of magnetic shielding coefficient is shown in formula (1) :

$$S = \frac{B_e}{B_i} \quad (1)$$

Where, B_e is the magnetic induction intensity before shielding, unit: T; B_i is the magnetic induction intensity after shielding, unit: T. After calculating this shielding factor, the magnetic shielding factor of $Fe_{15}Ni_{80}Mo_4Si_1$ material can reach 1.5×10^9, which is 145% higher than that of the conventional 1J85 material with 300,000 permeability.

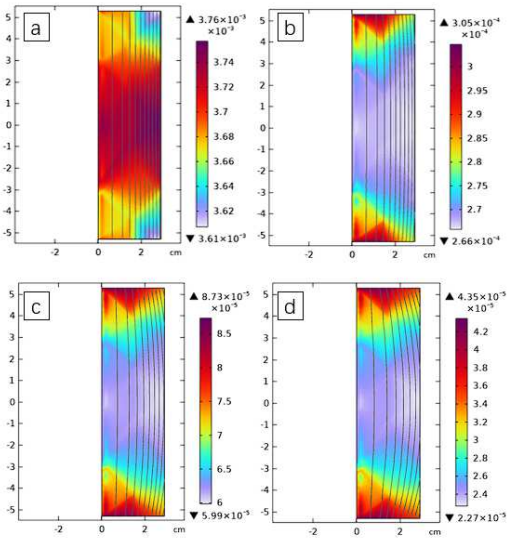

Fig. 6. The magnetic field distribution in the storage bubble under different permeability is (a) μ= 100,000 (b) μ= 200,000 (c) μ= 300,000 (d) μ= 400,000

TABLE II. MAGNETIC SHIELDING EFFECT

Permeability μ	Magnetic field B (nT)	Magnetic shielding factor S
100000	3.7×10-3	1.1×107
200000	2.7×10-4	1.5×108
300000	6.6×10-5	6.1×108
400000	2.8×10-5	1.4×109
407584	2.6×10-5	1.5×109

C. *Influence of Permeability on the Number of Shielding Layers*

At present, the thickness of the magnetic shield layer of the hydrogen frequency is mainly 0.5 mm and 1 mm. Fig.7 shows the internal magnetic field of the three-layer shield shell with a thickness of 1 mm when the permeability is 407584. The average internal magnetic field size is 8.8×10^{-4} nT, and the magnetic shielding coefficient is 4.5×10^{-7}, which is similar to that of the four-layer magnetic shielding when the permeability is 200,000, while the mass is increased by 1112 g, for 28.9%, and the volume is reduced by 4414 cm3, for 52%.

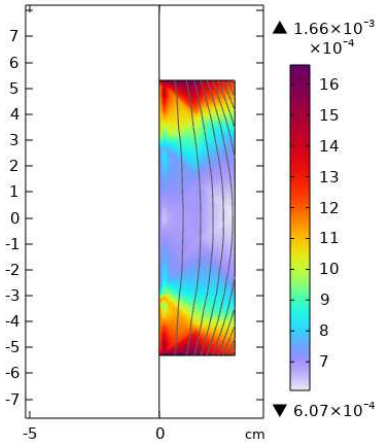

Fig. 7. Magnetic field distribution of the storage bubble area in a three-layer magnetic shield shell with a thickness of 1 mm

V. CONCLUSION AND DISCUSSION

This paper prepared a new permalloy and compared it with the one being used. After simulating the difference of magnetic shielding coefficient caused by different materials through software, the following conclusions were finally reached:

1) In $Fe_{15}Ni_{80}Mo_{(5-x)}Si_x$ (x= 0,1,2,3) alloy, the grain size continues to increase with the increase of Si content. When the Si content is more than 1, Si becomes the nucleation point, and smaller grains appear in the grains, and the uniformity becomes worse. The $FeNi_3$-phase (200) and (220) oriented grains grew preferentially with the increase of Si content. The permeability of $Fe_{15}Ni_{80}Mo_4Si_1$ can reach 407584, which is much higher than the permeability of the currently used 1J85 material.

2) The internal magnetic field size of the magnetic shield system is simulated under different permeability. When the permeability increases from 100000 to 407584, the magnetic shielding coefficient increases from 1.1×10^7 to 1.5×10^9. When the permeability is 407584, under the condition of reducing the number of layers and thickening the thickness of the magnetic shielding material, the magnetic shielding coefficient when the permeability is 200000, the mass will increase by 28.9% and the volume will be reduced by 52%.

In the future, different materials will also be considered to act as different shielding layers to cope with the requirements of AC magnetic fields and corrosion-prone environments. At the same time, the microstructure of 1J85 alloy can also be more uniform in the direction of improvement, the focus is still on the composition and heat treatment process.

REFERENCES

[1] Pan Zhibing, Xie Yonghui, Shuai Tao, et al. Application of a new high performance magnetic shielding system on a passive hydrogen atom clock [J]. Journal of Time and Frequency, 2021, 44(1): 45-54.

[2] Daniel Kleppner, H. Mark Goldenberg, Norman F. Ramsey, Theory of the Hydrogen Atom Clock, Physical Review, Volume 126, Number2, April 15 ,1962

[3] Leitner H, Schober M, Clemens H, Caliskanoglu D, Danoix F. Precipitation behaviour of an Fe-Co-Mo-alloy during nonisothermal ageing. Int J Math Res 2008;99:367-374.

[4] Eidenberger E, Stergar E, Leitner H, Staron P, Spitaler J, Ambosch-Draxl C, et al. Combined use of small-angle neutron scattering and atom probe tomography for the analysis of precipitates in a Fe-15m%Co-25m%Mo alloy. Appl Phys A 2009;97:331-340.

[5] Chenghui Lei, Bing Wang, Yue Chen, Effect of heat treatment on ac and dc magnetic properties of high permeability soft magnetic alloys 1J85, Procedia Engineering 27 (2012) 652 – 657

[6] A. A. Belyaev, S. A. Kozlov, A. A. Ul'yanov, Experimental investigation of a passive hydrogen frequency standard, March 1984.Measurement Techniques 27(3):224-226

[7] Sun S C, Mu J W, Jiang Z H, Ji C T, Lian J S, Jiang Q. Effect of cold rolling on tensile properties and microstructure of high nitrogen alloyed austenitic steel [J]. Materials Science and Technology, 2014, 30(2): 146-151.

[8] Tirumalasetty G K, Huis M A, Kwakernaak C, Sietsma J, Sloof W G, Zandbergen H W. Deformation-induced austenite grain rotation and transformation in TRIP-assisted steel [J]. Acta Materialia, 2012, 60(3): 1311-1321.